

Precise Characterization of ${}^6\text{Li}$ Feshbach Resonances Using Trap-Sideband-Resolved RF Spectroscopy of Weakly Bound Molecules

G. Zürn,^{1,2} T. Lompe,^{1,2,3,*} A. N. Wenz,^{1,2} S. Jochim,^{1,2,3} P. S. Julienne,⁴ and J. M. Hutson^{5,†}

¹*Physikalisches Institut, Ruprecht-Karls-Universität Heidelberg, 69120 Heidelberg, Germany*

²*Max-Planck-Institut für Kernphysik, Saupfercheckweg 1, 69117 Heidelberg, Germany*

³*ExtreMe Matter Institute EMMI, GSI Helmholtzzentrum für Schwerionenforschung, 64291 Darmstadt, Germany*

⁴*Joint Quantum Institute, NIST and the University of Maryland, Gaithersburg, Maryland 20899-8423, USA*

⁵*Department of Chemistry, Joint Quantum Centre (JQC) Durham/Newcastle, Durham University, South Road, Durham, DH1 3LE, United Kingdom*

We perform radio-frequency dissociation spectroscopy of weakly bound ${}^6\text{Li}_2$ Feshbach molecules using low-density samples of about 30 molecules in an optical dipole trap. Combined with a high magnetic field stability this allows us to resolve the discrete trap levels in the RF dissociation spectra. This novel technique allows the binding energy of Feshbach molecules to be determined with unprecedented precision. We use these measurements as an input for a fit to the ${}^6\text{Li}$ scattering potential using coupled-channel calculations. From this new potential, we determine the pole positions of the broad ${}^6\text{Li}$ Feshbach resonances with an accuracy better than 7×10^{-4} of the resonance widths. This eliminates the dominant uncertainty for current precision measurements of the equation of state of strongly interacting Fermi gases. As an important consequence, our results imply a corrected value for the Bertsch parameter ξ measured by Ku et al. [Science 335, 563 (2012)], which is $\xi = 0.370(5)(8)$.

PACS numbers: 67.85.-d

In the past few years, ultracold Fermi gases of neutral atoms have become important benchmark systems for testing theories of strongly interacting many-body systems [1]. This success is based on two main factors. The first is that the physics of ultracold gases is very well approximated by simple model Hamiltonians. These Hamiltonians contain only a contact interaction, which can be described by a single quantity, the scattering length a . The second is the existence of Feshbach resonances in the interparticle scattering, which cause the scattering length to diverge to $\pm\infty$ at certain magnetic field values B_0 [2]. This allows tuning of the interparticle interactions by applying a homogeneous magnetic offset field. Using such resonances, the properties of strongly interacting Fermi gases have been investigated using a number of different techniques, which range from radio-frequency (RF) spectroscopy [3, 4], through studies of collective oscillations [5, 6], to the detailed analysis of in-trap density profiles [7–9]. However, regardless of which technique is used, all such measurements depend on accurate knowledge of the properties of the Feshbach resonance that is used to tune the interactions.

${}^6\text{Li}$ atoms in the three energetically lowest Zeeman sub-levels of the electronic ground state (labeled $|1\rangle$, $|2\rangle$ and $|3\rangle$ following Ref. [10]) are widely used to realize strongly interacting Fermi gases. The interactions between atoms in the three different spin states are described by three scattering lengths a_{12} , a_{23} and a_{13} , which can all be tuned using broad Feshbach resonances located at magnetic fields of about 800 G with resonance widths of up to 300 G [33]. These resonances have been used to create the best known realization of a Fermi gas with diverging scattering length, which is a valuable benchmark system

for many-body theories. How well this benchmark system can be realized is currently limited by the accuracy of the previous determination of the resonance positions, which was $\lesssim 1.5$ G [10]. Recent studies of the equation of state (EoS) of strongly interacting Fermi gases have reached a level of precision at which they are limited by these uncertainties in the resonance positions. An important example is measurements recently performed by Nascimbéne et al. [7] and Ku et al. [9] with the goal of measuring the EoS at the point where the scattering length diverges to $\pm\infty$. In this so-called unitary limit the scattering length drops out of the problem, leaving the interparticle spacing as the only remaining length scale. At zero temperature this has the consequence that all extensive quantities of the unitary Fermi gas are given by their values for a noninteracting system rescaled by a universal numerical constant ξ , known as the Bertsch parameter [11]. Ku et al. determined this parameter to be $\xi = 0.376 \pm 0.004$, providing a precision measurement that can serve as a test for theories in such different fields as cold gases, nuclear physics and the physics of neutron stars. However, if the measurement is performed at a finite value of the scattering length, it leads to systematic errors. The error in ξ resulting from the 1.5 G uncertainty in the resonance position determined by Bartenstein et al. is about 2% and is the largest error contribution [9]. This clearly illustrates the necessity of a new, more accurate determination of the properties of the ${}^6\text{Li}$ Feshbach resonances.

In this work we determine the positions of the broad ${}^6\text{Li}$ Feshbach resonances with an accuracy of 80 mG, which corresponds to less than 7×10^{-4} of the resonance widths. To achieve this we make use of the fact that

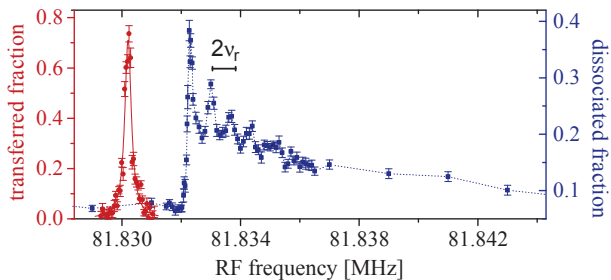


FIG. 1: RF spectra for the free-free (red dots, left axis) and bound-free (blue squares, right axis) spectra at a magnetic field of $B = 811.139$ G. The line shape of the free-free transition is well described by a Lorentzian (solid line). The bound-free spectrum shows distinct peaks spaced by $2\nu_r$, corresponding to different radial trap levels. The errors are the standard errors of the mean of about 40 individual measurements.

every Feshbach resonance is related to a weakly bound dimer state. Close to the resonance the binding energy of the dimer is approximately related to the scattering length by the universal relation $E_b = \hbar^2/ma^2$, where m is the mass of one atom [2]. Thus we can obtain information about the ${}^6\text{Li}$ Feshbach resonances by measuring the binding energy of such a weakly bound dimer state for different values of the magnetic field. However, the universal relationship is not accurate enough for quantitative interpretation, and in the present work we fit the measured binding energies to determine a new model interaction potential for ${}^6\text{Li}$ using coupled-channel calculations. This new potential in turn provides $a(B)$ as a function of magnetic field B and allows us to characterize the Feshbach resonances to high precision.

The most precise method currently available to measure the binding energy of these dimers is RF spectroscopy [10, 12]. This technique is based on applying an RF pulse to a gas of atoms to drive them from an initial hyperfine state $|i\rangle$ to a final state $|f\rangle$. For a sample of molecules one can either drive a transition to another weakly bound dimer state (bound-bound transition) or dissociate the dimer into two free atoms (bound-free transition). In either case the transition frequency is shifted from the free-free transition by the difference in the binding energies of the initial and final states. However, the transition frequency is also affected by the difference in the mean-field energies of the initial and final states. To avoid this systematic error, measurements of the dimer binding energy must be performed in a regime where the scattering length is much smaller than the interparticle spacing, i.e. $na^3 \ll 1$. In previous experiments this could be achieved only for relatively small values of $a \lesssim 2000 a_0$, as the experimentally achievable densities were limited to $n \gtrsim 10^{13}$ molecules/cm 3 . Accordingly, the smallest binding energies that could be measured were on the order of $E_b \simeq \hbar \times 100$ kHz, which resulted in a large uncertainty in the fitted resonance position.

We use the techniques we have developed to prepare and detect few-particle systems [13] to create very dilute samples of molecules. This allows us to perform RF spectroscopy of dimers with much smaller binding energies, and thus measure much closer to the resonance. We start from a small Bose-Einstein condensate of about 10^3 [12] molecules, trapped in a small-volume optical dipole trap at a magnetic field of 760 G. Subsequently we reduce the particle number to about 30 molecules by applying the spilling technique developed in Ref. [13]. We then superimpose a large-volume optical dipole trap with trap frequencies of $\nu_r = \omega_r/2\pi = 349(3)$ Hz and $\nu_{ax} = \omega_{ax}/2\pi = 35(1)$ Hz in the radial and axial directions, respectively. To transfer the molecules into this shallow dipole trap we suddenly switch off the microtrap. This nonadiabatic release results in a mean kinetic energy per particle of $\geq 0.4 \mu\text{K}$ and therefore a final molecular peak density of $n \leq 10^9$ molecules/cm 3 which greatly reduces density-dependent shifts of the RF transition [14].

To measure the bound-free spectra we first perform a 10 ms ramp from the magnetic field of 760 G at which

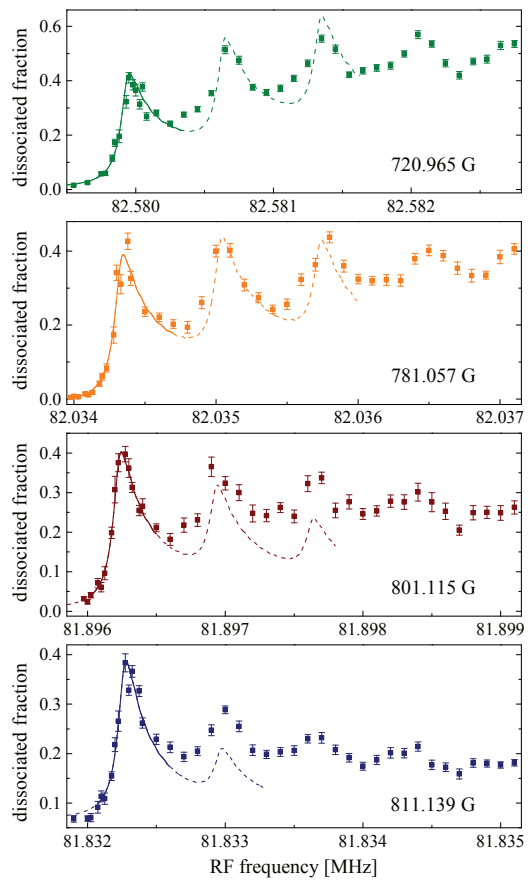


FIG. 2: Molecular dissociation spectra at four different magnetic fields. The lines show fits according to the model described in the text, with the solid parts indicating the range of the data points included in the fit.

Magnetic field B (stat.) (G)	Free-free transition ν_{ff} (stat.) (MHz)	Bound-free transition ν_{bf} (stat.)(sys.) (MHz)	Dissociation frequency $\nu_{\text{bf}} - \nu_{\text{ff}}$ (stat.)(sys.) (kHz)	Confinement shift $\nu_{\text{cs}} = \nu_0(\text{sys.}) + \nu_1(\text{sys.})$ (kHz)	Binding energy/ h ν_{E_b} (stat.)(sys.) (kHz)
811.139 (1)	81.830 115 (3)	81.832 271 (7)(8)	2.156 (8)(16)	0.367(3) - 0.014(1)	1.803 (8)(17)
801.115 (5)	81.891 539 (33)	81.896 236 (3)(8)	4.697 (33)(16)	0.367(3) - 0.011(1)	4.341 (33)(17)
781.057 (1)	82.019 823 (1)	82.034 336 (6)(8)	14.513 (6)(16)	0.367(3) - 0.011(1)	14.157 (7)(17)
720.965 (1)	82.452 482 (2)	82.579 943 (13)(8)	127.461 (13)(16)	0.367(3) - 0.021(1)	127.115 (14)(17)

TABLE I: Measured frequencies and resulting binding energies at different magnetic fields. The dissociation frequency $\delta\nu$ is obtained by subtracting the free-free transition frequency ν_{ff} from the bound-free transition frequency ν_{bf} . To obtain the binding energy we subtract the confinement induced frequency shift ν_{cs} from the dissociation frequency $\delta\nu$. The different contributions to the confinement induced shift ν_{cs} and the statistical (stat.) and systematic (sys.) errors are discussed in the Supplemental Material [14].

we prepare the sample to the magnetic field of interest and wait for another 5 ms. This time is long enough for the magnetic offset field to stabilize to an uncertainty of typically 1 mG, but short enough to avoid collisional dissociation of a significant fraction of molecules. We then apply a rectangular RF pulse of 10 ms duration to dissociate a fraction of the $|12\rangle$ molecules into free atoms in states $|1\rangle$ and $|3\rangle$. By measuring the number of these unbound atoms as a function of the RF frequency, we obtain spectra as shown by blue dots in Fig. 1. To limit saturation effects, we choose the pulse power such that we dissociate at most 30% to 40% of the molecules.

To measure the frequency of the free-free transition we prepare a spin-polarized Fermi gas of atoms in state $|2\rangle$ and drive the RF transition to state $|3\rangle$ (red dots in Fig. 1). We do this before and after the molecule dissociation measurement and use the weighted mean ν_{ff} of the two measurements [14]. From this we can also determine the magnetic field using the Breit-Rabi formula.

The profile of the bound-free spectrum is determined by the overlap between the wave functions of the initial molecular state ψ_i and of the accessible final states ψ_f [15]. As the RF photons carry only negligible momentum, there is no net momentum transfer to the system and therefore the RF pulse can affect only the relative motion of the two atoms. The transition rate between the initial and final state is thus proportional to $|\langle\psi_i(r)|\psi_f(r)\rangle|^2$, where r is the distance between the two atoms. For a continuum of final states the resulting asymmetric line shape is given by the momentum distribution of the initial molecular state [15]. In a confining potential, however, the final states are the discrete energy levels of the trap and the profile is determined by the overlap between the molecular state and the trap states. If the experimental resolution is insufficient to resolve the trap levels, as was the case in previous experiments [3, 4, 10, 12], the final state can be well described by a continuum. In our case the resolution is high enough to resolve the radial trap levels (see Fig. 2).

For the initial molecular state, the long-range part of the wave function for the relative motion is well described

by $\psi_i(r) \simeq e^{-r/a}$, where a is the scattering length. The final states are the levels of our optical trap, which we approximate as harmonic oscillator levels. Since the initial state is symmetric, only the symmetric harmonic oscillator levels ($n_{\text{ho}}=0,2,4,\dots$) contribute. Calculating the wave function overlap results in a spectrum of delta functions of different heights located at $\nu_{\text{bf}} + p\nu_r + q\nu_{\text{ax}}$, where ν_{bf} is the frequency of the bound-free transition and p, q are non-negative even integers. To fit our measured spectra, we convolute this spectral function with the line shape of the free-free transition, which we approximate by a Lorentzian with a FWHM of 122 Hz. Because of this finite resolution only the radial peaks are resolved. The free parameters of the fits are ν_{bf} , the overall amplitude, and a small offset in the atom number arising from collisional dissociation of molecules [16]. To determine ν_{bf} we fit the lowest radial peak at each field (solid lines in Fig. 2) [34]. The molecular binding energies, obtained by subtracting the confinement-induced frequency shifts [14, 17] from the dissociation frequencies $\nu_{\text{bf}} - \nu_{\text{ff}}$, are given in table I.

To fit the experimental results and extract the position of the broad resonance pole, we use a coupled-channel model similar to that of Refs. [18] and [10]. The interaction potentials are constructed using the short-range singlet potential of Ref. [19] and the short-range triplet potential of Ref. [20], joined at long range onto potentials based on the dispersion coefficients of Ref. [21] and the exchange function of Ref. [19]. The interatomic spin-dipolar interaction is taken to follow its long-range (r^{-3}) form at all distances. The singlet and triplet scattering lengths are adjusted by making small changes to the repulsive walls of the singlet and triplet potentials with parameters S_0 and S_1 . Scattering calculations are carried out using the MOLSCAT package [22], and bound-state calculations using the companion package BOUND [23, 24]. MOLSCAT can converge directly on the positions of poles and zeroes in the scattering length. We carried out least-squares fits to the new binding energy measurements described above, together with the two bound-bound spectroscopic frequencies of Ref. [10] at 661.436 G

	Fit Ref. [10]	Present fit	Experiment
$\nu_{b,12} - \nu_{b,13} + \nu_{ff}$ at 661.436 G	83 664.0(10)	83 665.9(3)	83 664.5(10)
$\nu_{b,12} - \nu_{b,13} + \nu_{ff}$ at 676.090 G	83 297.3(10)	83 297.3(3)	83 296.6(10)
$\nu_{b,12}$ at 720.965 G		127.115(17)	127.115(31)
$\nu_{b,12}$ at 781.057 G		14.103(26)	14.157(24)
$\nu_{b,12}$ at 801.115 G		4.342(17)	4.341(50)
$\nu_{b,12}$ at 811.139 G		1.828(11)	1.803(25)
Zero in a_{12}		527.32(25)	527.5(2)[25]
Narrow pole in a_{12}		543.41(12)	543.286(3)
a_s	45.167(8)	45.154(10)	[26]
a_t	-2140(18)	-2113(2)	

	pole (G)		Δ (G)		a_{bg} (a_0)	
	Ref.[10]	Present fit	Ref.[10]	Present fit	Ref.[10]	Present fit
[12]	834.15	832.18(8)	300	-262.3(3)	-1405	-1582(1)
[13]	690.43	689.68(8)	122.3	-166.6(3)	-1727	-1770(5)
[23]	811.22	809.76(5)	222.3	-200.2(5)	-1490	-1642(5)

TABLE II: Quality of fit between coupled-channel calculations on the best-fit two-parameter ${}^6\text{Li}$ potential and the experiments, together with key derived quantities calculated using the potential. The quantities in parentheses are estimates of the model dependence, including the effect of the systematic errors in the binding energies in Table I. All frequencies are given in kHz, all lengths in bohr and all magnetic fields in G. The Δ and a_{bg} values are obtained from local fits to $a(B)$ near the resonance and do not correctly reproduce the positions of the zeroes in $a(B)$.

and 676.090 G, the magnetic field near 527 G where the scattering length passes through zero [25], and the position of the narrow resonance near 543 G [26]. The least-squares fits were carried out using the interactive package I-NoLLS [27].

A two-parameter fit using only S_0 and S_1 proved capable of giving a good fit to all the experimental results except the position of the narrow resonance. This fit placed the narrow resonance about 0.12 G to high field of its experimental position. This discrepancy could be resolved by introducing a third parameter in a variety of ways, such as scaling the exchange potential or changing the value of the exponent parameter β in the exchange potential. However, in the absence of a good theoretical justification for the extra parameters, and since introducing them had little effect on the parameters of the resonances near 800 G, we ultimately chose a two-parameter fit, excluding the data point for the pole of the narrow resonance, as the most reliable for our purpose. To estimate the uncertainties in the pole positions and derived parameters, we repeated the fits using binding energies at the upper and lower limits of the systematic uncertainties and used the range of predictions from the various fits to estimate the model dependence.

The quality of fit and the key quantities calculated from the best-fit (two-parameter) potential are summarized in Table II. Tabulations of $a(B)$ for the best-fit potential are given in the Supplemental Material [14].

With these results, the uncertainty in the positions of the broad ${}^6\text{Li}$ Feshbach resonances is no longer a limiting factor for current experiments. Using our new calibration of $a(B)$ it is possible to address systematic errors in recent experiments which were caused by the inaccuracy of the previous determination of the resonance positions. The most striking example of this is the determination of the Bertsch parameter ξ by Ku et al. [9], which was performed using a mixture of ${}^6\text{Li}$ atoms in states $|1\rangle$ and $|2\rangle$ at a magnetic field of 834.15 G. At this field, our best-fit potential gives $a(B) = -2.124(80) \times 10^5 a_0$ and effective range $r_{\text{eff}} = 87.03(1) a_0$. The difference between the EoS at unitarity and the EoS measured at this finite value of the scattering length may be obtained by using Tan's contact $C(a)$ [9, 28]. This gives a corrected value for the normalized zero-temperature chemical potential μ/E_F at unitarity, which in turn gives a revised value of the Bertsch parameter $\xi = 0.370(5)(8)$ [29]. Here the first parenthesis denotes the statistical error, while the second gives the systematic uncertainty of the corrected value [35].

In this work we have established a new technique to measure the binding energy of weakly bound molecules by performing trap-sideband-resolved RF spectroscopy. By creating very dilute samples of molecules we have greatly reduced density-dependent shifts of the RF transitions, which has allowed us to perform spectroscopy of extremely weakly bound molecules. Using these techniques we have measured the binding energy of ${}^6\text{Li}$ Feshbach molecules with binding energies as low as $h \times 2$ kHz with an accuracy better than $h \times 50$ Hz, which is a 40-fold improvement compared to previous measurements [10]. From these binding energies we have determined the positions of the broad ${}^6\text{Li}$ Feshbach resonances with an accuracy of 80 mG using a coupled-channels calculation. This removes one of the major limiting factors for precision studies of strongly interacting Fermi gases.

The authors thank M. Ku and M. Zwierlein for providing the corrected value of ξ as well as enlightening discussions. The authors gratefully acknowledge support from IMPRS-QD, Helmholtz Alliance HA216/EMMI, the Heidelberg Center for Quantum Dynamics, ERC Starting Grant No. 279697, EPSRC, AFSOR MURI Grant No. FA9550-09-1-0617, and EOARD Grant No. FA8655-10-1-3033.

* Electronic address: lompe@physi.uni-heidelberg.de

† Electronic address: J.M.Hutson@durham.ac.uk

- [1] I. Bloch, J. Dalibard, and W. Zwerger, Rev. Mod. Phys. **80**, 885 (2008).
- [2] C. Chin, R. Grimm, P. Julienne, and E. Tiesinga, Rev. Mod. Phys. **82**, 1225 (2010).
- [3] C. Chin, M. Bartenstein, A. Altmeyer, S. Riedl, S. Jochim, J. Hecker Denschlag, and R. Grimm, Science

- 305**, 1128 (2004).
- [4] C. H. Schunck, Y. Shin, A. Schirotzek, and W. Ketterle, *Nature* **454**, 739 (2008).
- [5] M. Bartenstein, A. Altmeyer, S. Riedl, S. Jochim, C. Chin, J. Hecker Denschlag, and R. Grimm, *Phys. Rev. Lett.* **92**, 203201 (2004).
- [6] J. Kinast, S. L. Hemmer, M. E. Gehm, A. Turlapov, and J. E. Thomas, *Phys. Rev. Lett.* **92**, 150402 (2004).
- [7] S. Nascimbéne, N. Navon, K. J. Jiang, F. Chevy, and C. Salomon, *Nature* **463**, 1057 (2010).
- [8] M. Horikoshi, S. Nakajima, M. Ueda, and T. Mukaiyama, *Science* **327**, 442 (2010).
- [9] M. J. H. Ku, A. T. Sommer, L. W. Cheuk, and M. W. Zwierlein, *Science* **335**, 563 (2012).
- [10] M. Bartenstein, A. Altmeyer, S. Riedl, R. Geursen, S. Jochim, C. Chin, J. Hecker Denschlag, R. Grimm, A. Simoni, E. Tiesinga, C. J. Williams, P. S. Julienne, *Phys. Rev. Lett.* **94**, 103201 (2005).
- [11] G. Baker, *Int. J. Mod. Phys. B* **15**, 1314 (2001).
- [12] C. A. Regal, C. Ticknor, J. L. Bohn, and D. S. Jin, *Nature* **424**, 47 (2003).
- [13] F. Serwane, G. Zürn, T. Lompe, T. B. Ottenstein, A. N. Wenz, and S. Jochim, *Science* **332**, 336 (2011).
- [14] See Supplemental Material. A table containing the scattering lengths $a(B)$ for the $|12\rangle$, $|13\rangle$ and $|23\rangle$ channels can be found at <http://www.lithium6.de/scatteringlengths.txt> or at <http://prl.aps.org/supplemental/PRL/v110/i13/e135301>.
- [15] C. Chin and P. S. Julienne, *Phys. Rev. A* **71**, 012713 (2005).
- [16] C. Chin and R. Grimm, *Phys. Rev. A* **69**, 033612 (2004).
- [17] Z. Idziaszek and T. Calarco, *Phys. Rev. A* **74**, 022712 (2006).
- [18] K. M. O'Hara, S. L. Hemmer, S. R. Granade, M. E. Gehm, J. E. Thomas, V. Venturi, E. Tiesinga, and C. J. Williams, *Phys. Rev. A* **66**, 041401(R) (2002).
- [19] R. Coté, A. Dalgarno, and M. J. Jamieson, *Phys. Rev. A* **50**, 399 (1994).
- [20] C. Linton, F. Martin, A. J. Ross, I. Russier, P. Crozet, A. Yiannopoulou, L. Li, and A. M. Lyyra, *J. Mol. Spectrosc.* **196**, 20 (1999).
- [21] Z. C. Yan, J. F. Babb, A. Dalgarno, and G. W. F. Drake, *Phys. Rev. A* **54**, 2824 (1996).
- [22] J. M. Hutson and S. Green (2011), MOLSCAT computer code.
- [23] J. M. Hutson (2011), BOUND computer code.
- [24] J. M. Hutson, E. Tiesinga, and P. S. Julienne, *Phys. Rev. A* **78**, 052703 (2008).
- [25] X. Du, L. Luo, B. Clancy, and J. E. Thomas, *Phys. Rev. Lett.* **101**, 150401 (2008).
- [26] E. L. Hazlett, Y. Zhang, R. W. Stites, and K. M. O'Hara, *Phys. Rev. Lett.* **108**, 045304 (2012).
- [27] M. M. Law and J. M. Hutson, *Comp. Phys. Comm.* **102**, 252 (1997).
- [28] S. Tan, *Ann. Phys.* **323**, 2971 (2008).
- [29] M. Ku and M. W. Zwierlein, private communication (2012).
- [30] G. Breit and I. I. Rabi, *Phys. Rev.* **38**, 2082 (1931).
- [31] see also G. Zürn, PhD thesis, Ruprecht-Karls-Universität Heidelberg (2012).
- [32] G. F. Gribakin and V. V. Flambaum, *Phys. Rev. A* **48**, 546 (1993).
- [33] Units of gauss rather than Tesla, the accepted SI unit of magnetic field, are used in this paper to conform to the conventional usage of this field.
- [34] As we chose to dissociate a relatively large fraction of the molecules ($\simeq 40\%$ for the first peak) to obtain a good signal-to-noise ratio for this fit, the absolute height of the peaks is affected by saturation. If the different peaks have similar heights, as is the case at $B = 781$ G, saturation affects them equally and the model shows quantitative agreement for all peaks. If the peak heights differ strongly the model shows only qualitative agreement for the peaks corresponding to final states with higher energy (dashed lines in fig. 2).
- [35] This systematic uncertainty is estimated from the difference between the corrected values for the chemical potential $\mu/E_F = 0.370$, energy $E/E_F = 0.362$ and free energy $F/E_F = 0.375$ of the unitary Fermi gas, which should all converge to ξ for $T \rightarrow 0$.

SUPPLEMENTAL MATERIAL

Determination of the dissociation frequency

To determine the dissociation frequency we measure the bound-free transition frequency ν_{bf} and the free-free transition frequency ν_{ff} . To check for shifts of the RF-transitions during the experiment we measure the free-free transition before (ν_{ff1}) and after (ν_{ff2}) the molecule dissociation measurement and use the weighted mean ν_{ff} of both measurements. The dissociation frequency is then given by $\delta\nu = \nu_{\text{bf}} - \nu_{\text{ff}}$. The magnetic field is calibrated by inserting ν_{ff} into the Breit-Rabi-Formula [30]. To determine the density dependent shift $\Delta\nu_{\text{density}}$ we increase the particle number from 30 to about 200 molecules. We find a shift of $\delta\nu$ which is smaller than 50 Hz, from which we estimate a shift of less than 0.125 Hz per particle in a linear approximation. Therefore the systematic uncertainty due to density effects is $\Delta\nu_{\text{density}} = 8$ Hz for a sample of 30 molecules (60 atoms). All parameters involved in the determination of the dissociation frequencies are listed in TABLE III.

Confinement shift

To determine the binding energy of the molecules we have to subtract the effects of the confining potential from the dissociation frequency $\delta\nu$. The main contribution to the confinement shift is the zero point energy E_0 of the relative motion of the dissociated particles in the trap which is given by the frequency $\nu_0 = \nu_r + \frac{1}{2}\nu_{ax} = 367(3)$ Hz. In the limit of vanishing scattering length, $a \rightarrow -0$, E_0 is the only contribution to the shift. For non-zero scattering length an exact expression for the energy of two particles in a cigar shaped harmonic trap with aspect ratio η has been derived in ref. [17]. It relates a to the total energy $E < E_0$ of the two particles

$$-\frac{1}{a} = \frac{1}{\sqrt{\pi}} \mathcal{F}(-\mathcal{E}/2). \quad (1)$$

with $\mathcal{E} = E - E_0$. The integral representation of $\mathcal{F}(x)$ is given by

$$\mathcal{F}(x) = \int_0^\infty dt \left(\frac{\eta e^{-xt}}{\sqrt{1 - e^{-t}}(1 - e^{-\eta t})} - \frac{1}{t^{3/2}} \right) \quad (2)$$

To calculate the energy we numerically solve equation 1. The result for an aspect ratio of $\eta = 10$ is shown in figure 3 (blue curve). The difference to the universal bound state in free space (green curve, [2]) determines the confinement shift.

To obtain the confinement shift of the initial state and

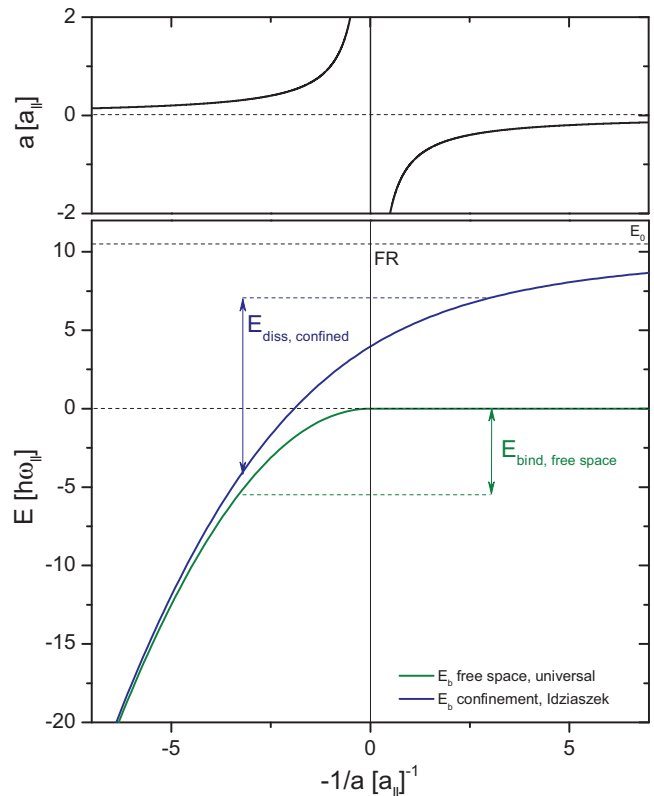


FIG. 3: **Confinement shift** [31]. The green curve shows the energy of the universal bound state associated with a Feshbach resonance [2]. At the point where the scattering length diverges at the Feshbach resonance (FR, upper panel) the universal bound state reaches the continuum. By measuring its binding energy in free space (green arrow) as a function of the magnetic field one can determine the position of the Feshbach resonance. The blue curve shows the universal bound state in the presence of the confinement ([17], $\eta = 10$). The blue arrow indicates an RF transition from a molecule at $a > 0$ to two atoms with $a < 0$. Due to the confinement the dissociation frequency is shifted with respect to the one in free space. The units are $\omega_{||} = 2\pi\nu_{ax}$ and $a_{||} = \sqrt{\frac{\hbar}{\mu\omega_{||}}}$.

the final state of the dissociation measurement at different magnetic fields we estimate the scattering length a_{12} from the corresponding dissociation frequencies. Therefore we first estimate the binding energy by subtracting ν_0 from the dissociation frequency. Then we calculate the scattering length using the expression of ref. [32] for the energy E_{gf} of the bound state which considers effective range corrections to first order

$$E_{\text{gf}} = \frac{\hbar^2}{\mu(a_{12} - \bar{a})^2} \quad (3)$$

with μ the reduced mass and with the so-called mean scattering length

$$\bar{a} \approx 0.487r_{\text{vdw}} \quad (4)$$

magn. field B [G]	free-free 1st ν_{ff1} [MHz]	free-free 2nd ν_{ff2} [MHz]	free-free weighted mean ν_{ff} [MHz]	bound-free transition ν_{bf} [MHz]	dissociation freq. $\delta\nu$ [kHz]
811.139 (1)	81.830 120 (8)	81.830 113 (5)	81.830 115 (3)	81.832 271 (7)(8)	2.156 (8)(16)
801.115 (5)	81.891 515 (3)	81.891 583 (4)	81.891 539 (33)	81.896 236 (3)(8)	4.697 (33)(16)
781.057 (1)	82.019 822 (2)	82.019 824 (3)	82.019 823 (1)	82.034 336 (6)(8)	14.513 (6)(16)
720.965 (1)	82.452 484 (4)	82.452 479 (5)	82.452 482 (2)	82.579 943 (13)(8)	127.461 (13)(16)

TABLE III: **Transition and dissociation frequencies [31].** The errors $\sigma_{\nu_{\text{ff1}}}$ and $\sigma_{\nu_{\text{ff2}}}$ of the measured free-free transition frequencies are the statistical errors of the fit to the free-free transition. $\nu_{\text{ff}} = \frac{\sum_i \frac{1}{\sigma_{\nu_{\text{ff}i}}^2} \nu_{\text{ff}i}}{\sum_i \frac{1}{\sigma_{\nu_{\text{ff}i}}^2}}$ is the weighted mean of ν_{ff1} and

ν_{ff2} with error $\sigma_{\nu_{\text{ff}}} = \sqrt{\frac{\sum_i \frac{1}{\sigma_{\nu_{\text{ff}i}}^2} (\nu_{\text{ff}i} - \nu_{\text{ff}})^2}{\sum_i \frac{1}{\sigma_{\nu_{\text{ff}i}}^2}}}$. The magnetic field error σ_B is the error resulting from the statistical error $\sigma_{\nu_{\text{ff}}}$.

For the bound-free transition frequency ν_{bf} the first parenthesis gives the statistical error $\sigma_{\nu_{\text{bf}}}$ of a Lorentzian fit to the rising slope of the first peak of the spectrum. The second parenthesis gives the systematic error $\Delta_{\nu_{\text{model}}}$ of the fit, which we estimate by the difference between the fitted frequency using either a Lorentzian lineshape or a Gaussian lineshape to describe the transition peak into a single trap sideband. For the dissociation frequency $\delta\nu$ the statistical error (first parenthesis) is obtained by quadratic addition of $\sigma_{\nu_{\text{ff}}}$ and $\sigma_{\nu_{\text{bf}}}$, while the systematic error is the sum of $\Delta_{\nu_{\text{model}}}$ and the systematic uncertainty due to density dependent shifts $\Delta_{\nu_{\text{density}}}$ (see text).

dissociation freq. $\delta\nu$ [kHz]	initial a a_{12} [10^3 bohr]	final a a_{13} [10^3 bohr]	initial cs shift $\nu_{\text{cs-i}}$ [kHz]	final cs shift $\nu_{\text{cs-f}}$ [kHz]	cs shift ν_{cs} [kHz]	binding energy/h ν_{E_b} [kHz]
2.156 (8)(16)	18.34	-3.54(1)	0.006	0.359(1)	0.353 (3)(1)	1.803 (8)(17) (25)
4.697 (33)(16)	11.80	-3.69(2)	0.002	0.358(1)	0.356 (3)(1)	4.341 (33)(17) (50)
14.513 (6)(16)	6.54	-4.10(3)	0.002	0.357(1)	0.356 (3)(1)	14.157 (7)(17) (24)
127.461 (13)(16)	2.20	-8.71(22)	0.000	0.346(1)	0.346 (3)(1)	127.115 (14)(17) (31)

TABLE IV: **Dissociation frequencies and binding energies [31].** The scattering length a_{12} is calculated using equation 3 and a_{13} is determined from $a_{13}(B)$ of ref. [10]. Its systematic error results from the 1 G uncertainty of the $|13\rangle$ pole in ref [10]. The confinement shift of the initial and final state of the rf-transition is calculated using equation 1. The error is the propagated error of a_{13} . The difference of both shifts determines the total confinement shift ν_{cs} . The first parenthesis states the statistical error of the zero point energy of the relative motion given by the SEM of the radial trap frequency which is determined from the separation of the sideband peaks in the dissociation spectra. The second parenthesis gives the systematic error of the confinement shift of the final state. The quadratic addition of both errors determines $\Delta_{\nu_{\text{cs}}}$. The binding energy E_b is calculated from the difference between the measured dissociation frequency and the confinement shift. The first parenthesis gives the statistical error $\sigma_{\nu_{E_b}}$ (see TABLE III). The second parenthesis gives the systematic error $\Delta_{\nu_{E_b}} = \Delta_{\nu_{\text{model}}} + \Delta_{\nu_{\text{density}}} + \Delta_{\nu_{\text{cs}}}$. The third parenthesis gives the sum of the statistical and systematic error.

where r_{vdw} is the range of the van-der-Waals potential. The scattering length a_{13} at the corresponding magnetic fields is taken from ref. [10]. The scattering length a_{12} of the initial state and a_{13} of the final state of the rf-

dissociation measurement and the corresponding confinement shifts are listed in TABLE IV. By subtracting the total confinement shift from the dissociation frequency we obtain the binding energy of a molecule in free space.